236 *Biochemistry* **2010,** *49,* 236–246
DOI: 10.1021/bi901725x

BIOCHEMISTRY
including biophysical chemistry & molecular biology
Article

Intermonomer Interactions Are Essential for Lysosomal Enzyme Binding by the Cation-Dependent Mannose 6-Phosphate Receptor[†,‡]

Linda J. Olson, Guangjie Sun, Richard N. Bohnsack, Francis C. Peterson, Nancy M. Dahms,* and Jung-Ja P. Kim*

Department of Biochemistry, Medical College of Wisconsin, Milwaukee, Wisconsin 53226

Received October 6, 2009; Revised Manuscript Received November 20, 2009

ABSTRACT: The 46 kDa cation-dependent mannose 6-phosphate receptor (CD-MPR) plays a key role in the delivery of lysosomal enzymes to the lysosome by binding newly synthesized mannose 6-phosphate (Man-6-P)-containing acid hydrolases and diverting them from the secretory pathway. Previous studies on a truncated form of the receptor comprised of only the soluble extracellular region (sCD-MPR, residues 1−154) have shown that the CD-MPR exists as a homodimer and exhibits two distinct conformations in the ligand-bound versus ligand-unbound states, involving changes in quaternary structure and positioning of loop D, the residues of which form a side of the binding pocket in the presence of ligand. To determine the role of intermonomer contacts in the functioning of the sCD-MPR, site-directed mutagenesis was used to generate a construct lacking a salt bridge (Glu19−Lys137) that tethers the N-terminal α-helix of one subunit to loop D of the other subunit in the ligand-bound form. Here we show by surface plasmon resonance analyses and NMR spectroscopy that the elimination of this intermonomer salt bridge significantly decreases the binding affinity of the mutant receptor (E19Q/K137M) toward lysosomal enzymes and Man-6-P. Analyses of the E19Q/K137M mutant receptor crystallized under various conditions revealed an altered quaternary structure that is intermediate between those observed in the ligand-bound and ligand-unbound states. Taken together, the results demonstrate a key role for intermonomer interactions in the structure and functioning of the CD-MPR.

The biogenesis of lysosomes requires the correct sorting of >60 acid hydrolases from their site of synthesis in the endoplasmic reticulum to their final destination in lysosomes (*1*). This targeting event is mediated by the 46 kDa cation-dependent mannose 6-phosphate receptor (CD-MPR)[1] and the 300 kDa cation-independent mannose 6-phosphate receptor (CI-MPR), the only two members of the P-type family of lectins (*2*−*4*). The two MPRs recognize phosphomannosyl residues on high-mannose-type *N*-glycans that serve to mark newly synthesized soluble acid hydrolases for delivery to endosomal/lysosomal compartments. The MPRs transport their cargo from the trans Golgi network (TGN) to endosomes where the acidic pH of the endosomal compartment facilitates disassembly of the complex. The released lysosomal enzymes are packaged into lysosomes, while the receptors either return to the Golgi or TGN via a retromer-assisted transport system (*5*) to repeat the process or move to the plasma membrane where the CI-MPR, but not the CD-MPR, functions to internalize exogenous ligands at the cell surface (*6*, *7*). Consistent with its role in intracellular trafficking, biochemical studies have confirmed that the CD-MPR displays strict pH dependence with respect to ligand binding, with optimal binding occurring at the pH of the TGN (pH ∼6.5) and little or no binding occurring at pH >7.4 or <5.5, corresponding to values found at the cell surface or endosome, respectively (*7*, *8*). Both the CI-MPR and CD-MPR are required to transport the entire repertoire of lysosomal enzymes to lysosomes, and a recent report indicates that the CD-MPR transports several lysosomal enzymes not recognized by the CI-MPR (*9*).

The CD-MPR is a type I membrane glycoprotein that exists as a homodimer, with each subunit containing a single Man-6-P binding site (*8*). We previously reported the crystal structure of the extracellular region comprising residues 1−154 of the CD-MPR (sCD-MPR) in the absence of ligand at pH 6.5 (*10*) which shows that the ligand-free form of the extracytoplasmic region of the CD-MPR crystallized as a dimer and maintained an overall topology similar to that of the ligand-bound form at pH 6.5 (*11*). Surprisingly, unlike other lectins that do not display any significant conformational change induced by ligand binding, a dramatic change in quaternary structure was revealed: the CD-MPR monomers undergo significant movements relative to each other, resulting in an open conformation in all structures containing ligand in the binding pocket, and a closed conformation found in all structures lacking bound carbohydrate (*10*, *12*). Accompanying this change in quaternary structure, one (i.e., loop D) of the two essential loops that comprise the binding pocket repositions itself in the absence of ligand to a location held by the carbohydrate ligand. Thus, the integrity of the binding site

[†]This work was supported by National Institutes of Health Grant R01DK42667 (to N.M.D. and J.-J.P.K.).
[‡]Deposited as Protein Data Bank entries 3K41, 3K42, and 3K43.
*To whom correspondence should be addressed. N.M.D.: Department of Biochemistry, Medical College of Wisconsin, 8701 Watertown Plank Rd., Milwaukee, WI 53226; telephone, (414) 955-4698; fax, (414) 955-6510; e-mail, ndahms@mcw.edu. J.-J.P.K.: Department of Biochemistry, Medical College of Wisconsin, 8701 Watertown Plank Rd., Milwaukee, WI 53226; telephone, (414) 955-8479; fax, (414) 955-6510; e-mail, jjkim@mcw.edu.
[1]Abbreviations: CD-MPR, cation-dependent mannose 6-phosphate receptor; CI-MPR, cation-independent mannose 6-phosphate receptor; TGN, trans Golgi network; Man-6-P, mannose 6-phosphate; Ni-NTA, nickel nitriloacetic acid; SPR, surface plasmon resonance; sCD-MPR, soluble form of the CD-MPR containing a single N-glycosylation site at Asn81; Glc-6-P, glucose 6-phosphate; endo H, endo-β-*N*-acetylglucosaminidase H; Con A, concanavalin A; rms, root-mean-square; HSQC, heteronuclear single-quantum coherence.

 Published on Web 11/23/2009 © 2009 American Chemical Society

is preserved as the side chains of three (Gln66, Arg111, and Tyr143) of the four amino acids essential for recognition of the mannose ring maintain their ligand binding position due to this reorientation of loop D (*10*, *12*).

A comparison of the ligand-free and ligand-bound crystal structures of the CD-MPR revealed a solvent accessible intermonomer salt bridge, Glu19 from the N-terminal α-helix of one monomer and Lys137 from loop D of the other monomer, present only in the ligand-bound form. It was hypothesized that disruption of this intermonomer salt bridge could contribute to the pH sensitive release mechanism of the CD-MPR (*12*). In this work, the contributions of the intermonomer salt bridge between Glu19 and Lys137 to the functioning of the CD-MPR were evaluated both biochemically and biophysically. A CD-MPR mutant (E19Q/K137M) containing two amino acid substitutions (Glu19 replaced with Gln and Lys137 replaced with Met) was generated and analyzed for its ability to bind (1) lysosomal enzymes by quantitative surface plasmon resonance measurements and (2) the monosaccharide, Man-6-P, by NMR spectroscopy. Furthermore, the crystal structure of E19Q/K137M was determined under different conditions. Taken together, the results demonstrate the critical role this ionic interaction plays in stabilizing a high-affinity binding pocket and further highlights a mechanistic rationale for how this receptor functions as a dimer to bind lysosomal enzymes. Furthermore, the results show that the CD-MPR is dynamic and suggest that the E19Q/K137M mutant structure represents an intermediate along the pathway of cargo loading and unloading.

EXPERIMENTAL PROCEDURES

Materials. The following reagents were obtained commercially as indicated: restriction endonucleases (New England Biolabs); *Pichia pastoris* wild-type strain X-33, *P. pastoris* expression vectors pGAPZαA and pPICZαA, T4 DNA ligase, BenchMark prestained protein ladder, and Zeocin (Invitrogen Corp.); glucose 6-phosphate, Man-6-P, and concanavalin A (ConA) Sepharose (Sigma); protein A−horseradish peroxidase conjugate (Amersham Biosciences); Immobilon P (Millipore); SuperSignal West Pico chemiluminescent substrate (Pierce Chemical Corp.); nickel nitrilotriacetic acid (Ni-NTA) agarose (Qiagen); amine coupling kits, surfactant P20, and CM5 research grade sensor chips (GE Healthcare); and detergent screening kit (Hampton Research). MTX 3.2 cells that overexpress human β-glucuronidase were generously provided by W. Sly (St. Louis University School of Medicine, St. Louis, MO). Phosphomannan from *Hansenula holstii* was a kind gift of M. E. Slodki (Northern Regional Research Center, Peoria, IL).

Generation of Constructs. Plasmids containing a glycosylation-deficient form of the extracytoplasmic domain (residues 1−154) of the bovine CD-MPR in which asparagine residues at positions 31, 57, 68, and 87 were replaced with glutamine (Figure 1) to eliminate four of the five potential N-linked glycosylation sites, leaving the N-glycosylation site at position 81 intact, with (sCD-MPRHis_6) (*13*) or without (sCD-MPR) (*14*) a C-terminal tag composed of six histidine residues were modified to contain two additional amino acid substitutions to eliminate the salt bridge located between the two subunits of the dimer. E19Q and K137M substitutions were generated by oligonucleotide-directed mutagenesis according to the method of Kunkel et al. as described previously (*15*). The following mutagenic oligonucleotides were used: 5′-TTT GTT GAT CTC CAC CAG GC-3′ for E19Q and 5′-ACA GTG GTT CTC ATA TTC AT-3′ for K137M. DNA sequencing by the Protein and Nucleic Acid Core Facility (Medical College of Wisconsin) confirmed the presence of the predicted sequences. Constructs lacking a His tag (sCD-MPR and E19Q/K137M) were cloned into the pPICZαA vector for expression in *P. pastoris* following methanol induction, whereas E19Q/K137MHis_6 was placed into the pGAPZαA vector, which utilizes the glyceraldehyde-3-phosphate dehydrogenase promoter for constitutive expression of recombinant proteins in *P. pastoris*.

Expression and Purification of sCD-MPR, E19Q/K137M, and E19Q/K137MHis_6 Constructs. cDNA constructs were linearized with either BspHI (His-tagged constructs) or SacI (nontagged constructs) and transformed into *P. pastoris* wild-type strain X-33 by electroporation. Zeocin-resistant transformants were selected on YPDS (1% yeast extract, 2% peptone, 2% dextrose, and 1 M sorbitol) following incubation at 30 °C. Positive clones utilizing the pGAPαA expression vector were inoculated in liquid medium (1% yeast extract, 2% peptone, and 2% dextrose), and cultures were harvested after growth for 3 days at 30 °C. Positive clones expressed using the pPICZαA system were first grown overnight at 28 °C in minimal medium [0.34% yeast nitrogen base without amino acids, 0.1 M potassium phosphate (pH 6.0), 38 mM ammonium sulfate, 4×10^{-5}% biotin, and 2% glycerol]. To induce expression of the recombinant protein, the cells were resuspended to an OD_{600} of 1 in the minimal medium described above in which glycerol was replaced with 0.5% methanol as the sole carbon source, and the cultures were harvested after growth for 2−3 days at 25 °C. Following removal of the cells by centrifugation, medium containing E19Q/K137MHis_6 was concentrated by filtration using Amicon stirred cells and then dialyzed extensively against metal binding buffer [20 mM Tris, 0.5 M NaCl, and 10 mM imidazole (pH 8.0)]. After dialysis, the medium was passed over a nickel (Ni-NTA) affinity column. After being washed, the column was eluted in a stepwise fashion using elution buffer [20 mM Tris and 0.5 M NaCl (pH 8.0)] containing 20, 50, 100, or 250 mM imidazole. Purification of the nontagged proteins (sCD-MPR and E19Q/K137M) involved dialysis of the concentrated medium against 50 mM imidazole (pH 6.5) and 150 mM NaCl prior to gel filtration using a Superdex 75 column (1.6 cm × 60 cm, GE Healthcare). The concentration of the purified protein was determined using the Bradford assay (Bio-Rad) with bovine serum albumin (BSA) as the standard.

Isotopically labeled protein was generated by substituting ammonium sulfate with [^{15}N]ammonium sulfate in the induction medium and used for NMR spectroscopic analyses. NMR spectral quality was dramatically improved by removal of the receptor's single *N*-glycan at position 81: purified protein was treated with endo-β-*N*-acetylglucosaminidase H (endo H, 5 milliunits, Roche Molecular Biochemicals) overnight, and the deglycosylated protein was again subjected to gel filtration using a Superdex 75 column to remove the majority of the cleaved oligosaccharide. Residual oligosaccharide, along with contaminating mannan, which is secreted by *P. pastoris* yeast, was removed via Con A Sepharose chromatography. Proteins for NMR analyses were then buffer exchanged into a solution containing 10 mM deuterated bis-Tris (pH 6.5) and 150 mM NaCl.

Purification of Human β-Glucuronidase. Human β-glucuronidase was collected from serum-free conditioned medium from cells that overexpress and secrete this lysosomal enzyme

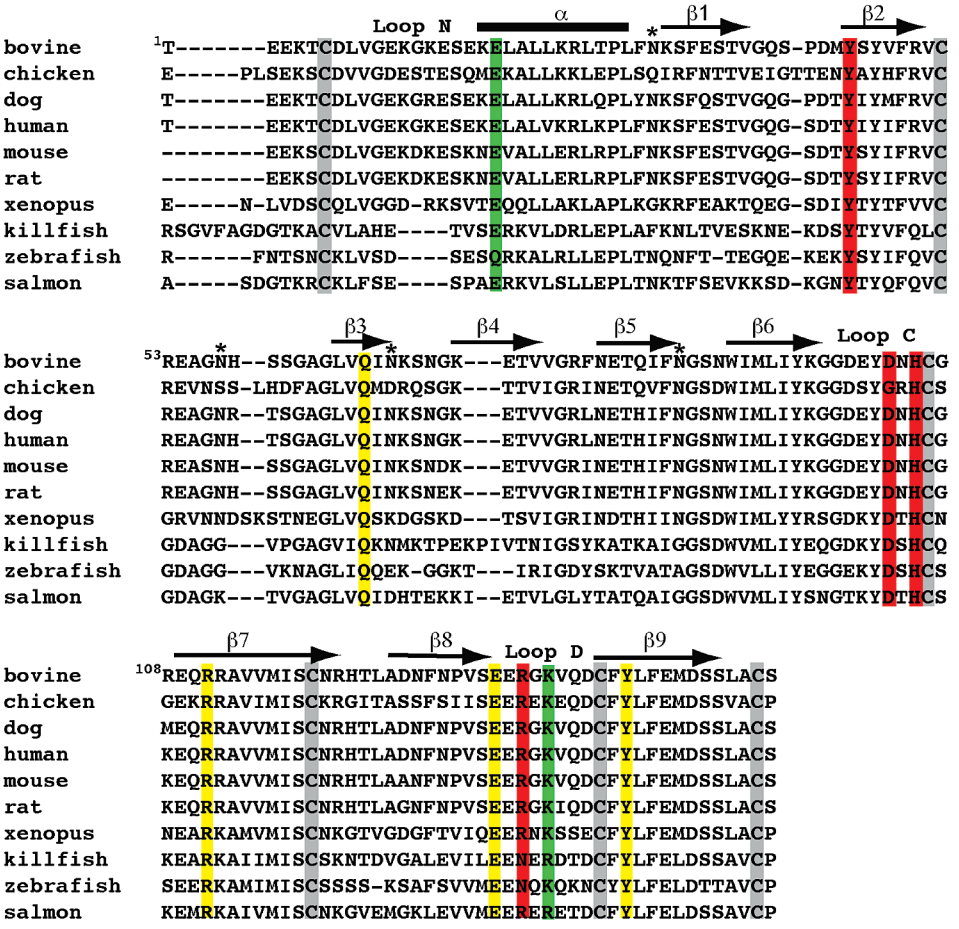

FIGURE 1: Amino acid sequence alignment of the extracytoplasmic region of the CD-MPRs from various species. The four N-glycosylation sites that have been mutated are indicated (asterisks). The secondary structure of the sCD-MPR is shown above the sequence with a cylinder representing the α-helix and arrows representing β-strands. The cysteine residues are boxed in gray. Residues that are within hydrogen bonding distance of Man-6-P are shown. The four residues essential for Man-6-P binding are highlighted in yellow, and residues that have been shown to have a modest [i.e., substitution of these residues results in a < 15-fold decrease in binding affinity (*13*)] effect on ligand binding are highlighted in red. The residues involved in an intermonomer salt bridge (Glu19 and Lys137) are highlighted in green.

(MTX 3.2 cells were generously provided by W. Sly. β-Glucuronidase was purified by affinity chromatography on a CI-MPR Affigel-10 column to remove nonphosphorylated enzyme as described previously (*16*).

Biosensor Studies. All SPR measurements were taken at 25 °C using a Biacore 3000 instrument (GE Healthcare). CM5 research grade sensor chips, surfactant P20, and amine coupling kits were also obtained from GE Healthcare. Purified proteins (sCD-MPRHis and E19Q/K137M) were immobilized on CM5 sensor chips following activation of the surface using 1-ethyl-3-[3-(dimethylamino)propyl]carbodiimide and *N*-hydroxysuccinimide as recommended by the manufacturer. Briefly, the proteins were injected onto the activated dextran surface at a concentration of 10−20 μg/mL in 10 mM sodium acetate buffer (pH 5.0) using immobilization buffer [10 mM MES (pH 6.5), 150 mM NaCl, and 0.005% (v/v) P20] as the running buffer. After coupling, unreacted *N*-hydroxysuccinimide ester groups were blocked with ethanolamine. The reference surface was treated in the same way except that protein was omitted. β-Glucuronidase was prepared in running buffer [50 mM MES (pH 6.5), 150 mM NaCl, 10 mM $MnCl_2$, 5 mM β-glycerophosphate, and 0.005% (v/v) P20] and was injected in a volume of 80 μL over the coupled and reference flow cells at a flow rate of 40 μL/min. After 2 min, the solution containing β-glucuronidase was replaced with buffer and the complexes were allowed to dissociate for 2 min. The sensor chip surface was regenerated with a 25 μL injection of 10 mM Man-6-P at a flow rate of 10 μL/min. The surface was allowed to re-equilibrate in running buffer for 1 min prior to subsequent injections. The sensorgrams were evaluated using BIAevaluation (version 4.0.1) and the K_d determined from a 1:1 Langmuir binding model (k_d/k_a). All response data were double-referenced (*17*), where controls for the contribution of the change in refractive index were performed in parallel with flow cells derivatized in the absence of protein and subtracted from all binding sensorgrams.

Protein Crystallization. The purified E19Q/K137MHis$_6$ and E19Q/K137M mutants were dialyzed extensively against buffer containing 50 mM imidazole (pH 6.5), 150 mM NaCl, 10 mM $MnCl_2$, and 5 mM β-glycerophosphate. E19Q/K137MHis$_6$ was preincubated with 10 mM Man-6-P for 1 h on ice prior to being used in crystallization experiments. Crystallization was conducted at 19 °C by vapor diffusion using the hanging drop method (*18*) by mixing equal volumes of the protein (13−15 mg/mL) solution with the well solution [for E19Q/K137MHis$_6$, 0.1 M cacodylate (pH 6.5), 25% polyethylene glycol (PEG) 2000 monomethyl ether, 0.2 M ammonium acetate, and 0.025 M octyl β-D-glucopyranoside (only in the drop); for E19Q/K137Msulfatep H7.0, 0.1 M HEPES (pH 7.0) and 3 M ammonium sulfate; for E19Q/K137MsulfatepH6.5, 0.1 M cacodylate (pH 6.5) and 3 M ammonium sulfate]. The E19Q/K137MHis$_6$ crystal was flash-frozen

after passing through a cryoprotection solution of the well solution with an additional 3% PEG as well as 20% glycerol added. The crystals from ammonium sulfate conditions were directly flash-frozen without any additional cryoprotectant. All diffraction data were collected at 100 K using an R-AXIS IV^{++} instrument equipped with a MicroMax007 generator and an Osmic mirror set. Data sets were processed with HKL2000 (*19*).

Structure Determination. The structures were determined using Amore in CCP4 (*20*) (E19Q/K137MHis$_6$) or Molrep (E19Q/K137MsulfatepH6.5) in CCP4i (*21*) using one monomer of the dimeric structure of the ligand-bound form of the CD-MPR [Protein Data Bank (PDB) entry 1C39] as the search model. In the case of E19Q/K137MsulfatepH6.5, the starting search model did not include residues 133−141 (loop D). The structure of E19Q/K137MsulfatepH7.0 was determined by the difference Fourier method using the E19Q/K137M model with residues 133−141 (loop D) omitted. Resulting models were refined using CNS (*22*) in conjunction with manual model adjustments using Turbo-Frodo (*23*). In the case of E19K137-MsulfatepH6.5, the twinning fraction (α = 0.284) and twinning operator (h, $-k$, $-l$) were calculated using CNS. The refinement was conducted again using CNS following protocols for treating partial hemihedral twinning. Data collection and refinement statistics for the final models are listed in Table 1.

Determination of Binding Affinities by Heteronuclear NMR Spectroscopy. NMR spectra were recorded on a Bruker 500 MHz spectrometer equipped with a triple-resonance CryoProbe and processed with NMRPipe software (*24*). [^{15}N]sCD-MPR and [^{15}N]E19Q/K137M were titrated with incremental additions of Man-6-P and monitored via two-dimensional (2D) ^{15}N−^{1}H heteronuclear single-quantum coherence (HSQC). Amide ^{1}H−^{15}N chemical shift perturbations were computed as $\Delta\delta = [(5\Delta\delta_H)^2 + \Delta\delta_N{}^2]^{1/2}$, where $\Delta\delta_H$ and $\Delta\delta_N$ are the changes in backbone amide ^{1}H and ^{15}N chemical shifts, respectively, in parts per million. Concentration-dependent changes in amide

Table 1: Data Collection and Refinement Statistics

	glycosylated	endoH-treated and conA-purified	
	EQKM/Man-6-P	EQKM/sulfatepH7.0	EQKM/sulfatepH6.5
PDB entry	3K41	3K42	3K43
pH	6.5	7.0	6.5
ligand/Mn[a]	M6P	−	−
Data Collection			
space group	$P2_12_12_1$	$I4$	$I4$[b]
cell dimensions a, b, c (Å)	53.2, 77.1, 79.9	102.6, 102.6, 100.1	103.0, 103.0, 99.8
wavelength (Å)	1.54	1.54	1.54
resolution (Å)	50.0−1.90 (1.97−1.90)	50−2.3 (2.38−2.3)	50−2.0 (2.07−2.0)
data collection temp (°C)	−175	−175	−175
R_{sym}	0.13 (0.53)	0.093 (0.481)	0.068 (0.41)
$I/\sigma I$	26.7 (3.6)	20.4 (3.7)	24.7 (4.6)
completeness (%)	99.8	99.9 (100.0)	99.7 (100.0)
redundancy	4.2	5.2	5.7
Refinement			
resolution (Å)	50−1.90	50−2.3	50−2.0
no. of reflections	25567	22239	344841
R_{work}/R_{free}	21.6/25.5	22.8/24.8	16.5/19.7
no. of monomers per asymmetric unit	2	2	2
residues present in each monomer	A4−A9, A16−A154 B4−B154	A3−A10, A15−A133, A141−A154 B5−B10, B15−B154	A3−A10, A15−A133, A141−A154 B5−B10, B16−B154
total no. of residues/B-average (Å^2)			
protein	304/26.2	287/30.3	286/29.8
M6P	2/22.5	−	−
NAG(Man)[c]	4(2)/49.6	2/47.9	2/35.0
water	161/33.9	187/36.1	199/35.6
sulfate	−	8/59.2	3/54.1
imidazole	0	0	1/39.4
acetate	0	0	1/39.6
glycerol 1-phosphate	0	2/47.2	0
rms deviations			
bond lengths (Å)	1.29	1.2	1.2
bond angles (deg)	0.006	0.006	0.006
Ramachandran plot (no. of residues/%)			
most favorable	221/85	200/80.0	213/85.5
additionally allowed	39/15	48/19.2	36/14.5
generously allowed	0/0	1/0.4	0/0
disallowed	0/0	1/0.4	0/0

[a]Although Mn^{2+} was present in the crystallization media for 120805 and 041509 crystals, no appreciable Mn^{2+} peak was found in either structure. [b]Twinned with $\langle I^2\rangle/\langle I\rangle^2$ = 1.645; twinning fraction of 0.284, and twinning operator (h, $-k$, $-l$). [c]Oligosaccharide attached to Asn81; NAG, *N*-acetylglucosamine.

chemical shift perturbations were fitted to the following equation that accounts for ligand depletion:

$$\Delta\delta = \frac{\Delta\delta_{max}}{2[\text{receptor}]} \times [K_d + [\text{receptor}] + x - (K_d + [\text{receptor}] + x)^2 - 4[\text{receptor}]x]^{1/2}$$

where $\Delta\delta$ represents the chemical shift perturbation, $\Delta\delta_{max}$ is the maximum chemical shift perturbation at 100% bound receptor, K_d is the apparent Man-6-P dissociation constant, and x is the Man-6-P concentration. K_d and $\Delta\delta_{max}$ values were obtained for each of the receptor residues by nonlinear curve fitting as previously described (*25*).

RESULTS AND DISCUSSION

The Mutant Form of the sCD-MPR Lacking an Intermonomer Salt Bridge Exhibits Decreased Binding Affinity for Lysosomal Enzymes. Previous comparative structural analyses of the sCD-MPR identified a solvent accessible intermonomer salt bridge (Glu19 from the N-terminal α-helix of one monomer and Lys137 from loop D of the other monomer) that was hypothesized to undergo protonation at acidic pH values, causing changes in quaternary structure and initiating a cascade of events that ultimately ends in the release of ligand (*12*). The observation that the region preceding Glu19 becomes disordered in structures determined under acidic pH conditions is consistent with this hypothesis (*12*). Furthermore, Glu19 and Lys137 are conserved in all species, with the exception of zebrafish in which Glu19 is replaced with Gln and killfish and salmon in which Lys137 is conservatively replaced with Arg (Figure 1). To determine whether the absence of this intermonomer salt bridge affects the binding affinity of the receptor for a lysosomal enzyme, β-glucuronidase, surface plasmon resonance (SPR) analyses were performed. The results demonstrate that sCD-MPR bound β-glucuronidase with high affinity (K_d = 26 nM) (Figure 2A), whereas no detectable binding was observed to E19Q/K137M at concentrations as high as 120 nM (Figure 2B). Consistent with these results, no detectable binding of E19Q/K137M was observed to a resin containing coupled phosphomannosyl residues (data not shown). In addition, two-dimensional $^{15}N-^{1}H$ HSQC NMR spectroscopy, which was used to measure the chemical shift perturbations upon addition of Man-6-P, revealed that EQKM bound Man-6-P with an ~150-fold lower affinity than sCD-MPR (see below). Taken together, the results show that the mutant's affinity for Man-6-P and β-glucuronidase is drastically compromised, demonstrating the essential role of the intermonomer salt bridge in the ability of the CD-MPR to bind lysosomal enzymes with high affinity.

Crystallization of a Mutant Form of the sCD-MPR Lacking an Intermonomer Salt Bridge. Two versions (i.e., with and without a C-terminal His_6 tag) of the mutant protein lacking an intermonomer salt bridge (E19Q/K137MHis$_6$ and E19Q/K137M) were crystallized and their structures determined (see Table 1). The presence of the His tag had no significant effect on the structure of the receptor (see below). Consistent with this observation are previous studies in which we demonstrated that sCD-MPRHis$_6$ bound the lysosomal enzyme, β-glucuronidase, with an affinity (K_d = 1.5 ± 0.2 nM) (*13*) that is comparable to that of the nontagged version of the receptor (sCD-MPR) expressed in *P. pastoris* (K_d = 1.4 nM) (*26*) and of the full-length receptor isolated from mammalian tissues [K_d = 0.28 nM (*7*); K_d = 4−5 nM (*27*)]. These results demonstrate that the presence of a C-terminal His tag does not alter the function of the sCD-MPR. Thus, hereafter, we refer to E19Q/K137MHis$_6$ and E19Q/K137M simply as "EQKM".

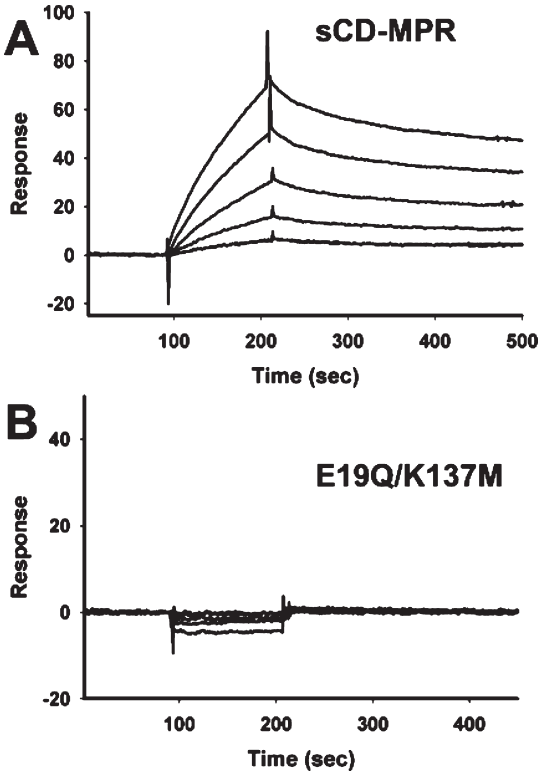

FIGURE 2: Interaction of sCD-MPR constructs with a lysosomal enzyme. SPR analysis of β-glucuronidase binding to immobilized sCD-MPR (A) and E19Q/K137M (B) constructs. sCD-MPR and E19Q/K137M were immobilized on the surface of a CM5 sensor chip to a level of 800 and 770 response units, respectively. β-Glucuronidase was injected in a volume of 80 μL over the sensor surface at a rate of 40 μL/min. After 2 min, the solution containing β-glucuronidase was replaced with buffer and the complexes were allowed to dissociate for 2 min. Various concentrations of β-glucuronidase (8, 10, 20, 40, 80, 100, and 120 nM) were injected over the immobilized receptors, and the resulting sensorgrams are shown.

Structures of two forms of EQKM have been obtained: (1) EQKM complexed with Man-6-P (EQKM/Man-6-P) and (2) EQKM crystallized in the absence of Man-6-P at pH 6.5 and 7.0. Each crystal form has one dimeric molecule in the asymmetric unit. As seen in other reported sCD-MPR structures (*10*−*12*, *28*), the overall fold of each monomer relative to the other monomer in the asymmetric unit is the same, with the rms deviation ranging from 0.25 to 0.32 Å for 122 to 143 Cα atoms, respectively. However, as observed with some previously determined sCD-MPR structures (*10*−*12*), one (monomer B) of the two monomers has fewer disordered residues. Thus, unless otherwise stated, monomer B was used for subsequent analyses.

Comparison of the Monomer Structure of EQKM/Man-6-P and sCD-MPR. The overall topology of the monomer polypeptide of EQKM/Man-6-P consists of a flattened β-barrel comprised of nine β-strands, with a short α-helix located at the amino terminus (Figure 3A). Comparative analyses revealed that the structure of the EQKM/Man-6-P monomer is essentially the same as that of the wild-type sCD-MPR monomer in the presence of ligand (rms deviation of 0.32 Å for 122 Cα atoms) (Figure 3A). Previous structures of the sCD-MPR have shown that the

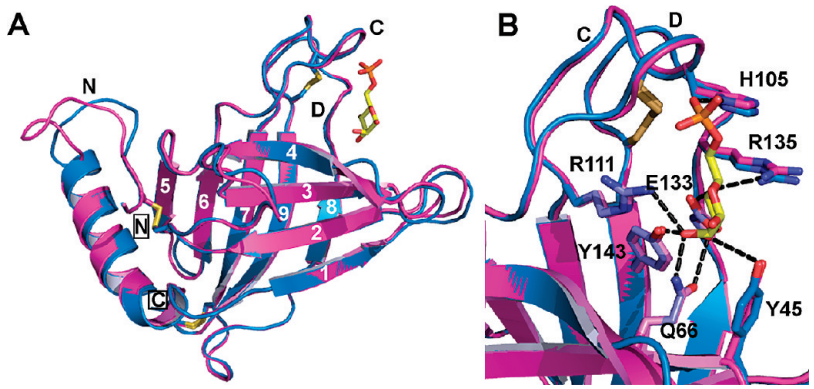

FIGURE 3: Superimposition of the monomer structure of the EQKM mutant and sCD-MPR. (A) The monomers of EQKM (cyan, PDB entry 3K41) and sCD-MPR (magenta, PDB entry 2RL8) crystallized in the presence of Man-6-P were compared. Loops N, C, and D are labeled, and the location of Man-6-P (yellow ball and stick) is shown. The N- and C-termini are boxed. β-Strands are numbered from 1 to 9. (B) Close-up view of the binding pocket. The seven amino acids involved in Man-6-P binding are labeled. Potential hydrogen bond interactions with Man-6-P are shown as black dashed lines.

carbohydrate binding pocket contains six residues (Tyr45, Gln66, Arg111, Glu133, R135, and Tyr143) that are within hydrogen bonding distance of the mannose ring hydroxyl groups and one residue (His105) that interacts with the phosphate moiety (Figure 3B) (*11*, *28*). These residues are conserved among species (Figure 1), and mutagenesis studies have demonstrated that four of these residues (Gln66, Arg111, Glu133, and Tyr143) are essential for Man-6-P binding as substitution of any one of these residues results in an ~1000-fold decrease in the receptors's binding affinity for a lysosomal enzyme (*13*, *15*). The architecture of the binding pocket, including the relative positions of these seven residues, is also preserved in the EQKM mutant in the presence of Man-6-P (Figure 3B). The only appreciable difference between the two monomer structures is the conformation of the N-terminal loop (Leu8−Lys14) and the first two amino acids (Glu15 and Ser16) of the α-helix that contains Gln19. However, the loop containing Lys137 (loop D, residues Glu133−Cys141) maintains the same conformation as wild-type sCD-MPR (Figure 3A). These comparative analyses indicate that disruption of the salt bridge between a residue in the N-terminal region and its partner located in loop D of the adjacent subunit does not influence the overall architecture of the Man-6-P binding pocket. Thus, the observed decrease in binding affinity for lysosomal enzymes by EQKM (Figure 2) does not appear to be due to a restructuring of the binding pocket but must arise from how one monomer associates with the other to form the dimer.

Comparison of the Dimer Structure of EQKM/Man-6-P and sCD-MPR. The CD-MPR functions as a dimer in the cell. Previous crystallographic studies have shown that the relative orientation of the monomers with respect to each other is dependent upon the presence or absence of ligands, rather than pH (*12*). In the absence of ligand, the receptor adopts a "closed" conformation with a reduced dimer interface area (1000 $Å^2$ open vs 770 $Å^2$ closed) that is due to loss of contacts between residues in loop D and residues near the N-terminus (residues Val9, Gly10, and Ser16−Lys18) of the other monomer. Interestingly, the ligand-bound structure of the salt bridge mutant (EQKM/Man-6-P) adopts a dimer conformation (Figure 4A,C) that appears to be "between" the previously described closed (ligand-free) and open (ligand-bound) structures of the sCD-MPR (Figure 4B,D). Specifically, the monomers of EQKM/Man-6-P are oriented with an ~20° scissor motion (10° per blade) away from the 2-fold axis (Z axis) on the $X-Z$ plane (Figure 4B) and an ~9° clockwise twist motion relative to that of the ligand-unbound form (Figure 4D). Relative to the ligand-bound form of the sCD-MPR, the monomers of EQKM/Man-6-P are oriented with an ~16° scissor motion (8° per blade) toward the 2-fold axis (Z axis) on the $X-Z$ plane (Figure 4B) and an ~9° counter-clockwise twist motion (Figure 4D). Although the ligand binding pocket architecture in the EQKM/Man-6-P structure is identical to that of sCD-MPR (Figure 3B), the interactions between the residues of the binding pocket and the neighboring residues that support the binding pocket are very different. The sCD-MPR structure reveals that the binding cavity is stabilized by interactions between loop D of one monomer and the residues within the N-terminal region of the other monomer, which includes electrostatic interactions and hydrogen bonds (Glu19−Lys137, Lys18−Glu134, and Ser16−Glu134) (Figure 4F). The absence of the salt bridge, Glu19−Lys137, in EQKM disrupts these intermonomer ionic interactions, resulting in a less stable binding pocket (Figure 4E), which in turn results in a >100-fold decrease in EQKM's ligand binding affinity (see Figures 2 and 5B).

Influence of Ligand Binding on the Solution Structure of EQKM and sCD-MPR. To further investigate the dynamic nature of the CD-MPR as inferred by the various crystal structures of the receptor (Figure 4B,D), the solution structures of sCD-MPR and EQKM were investigated by NMR spectroscopy. Two-dimensional $^{15}N-^{1}H$ HSQC spectra were collected for sCD-MPR and EQKM in the presence and absence of Man-6-P and compared. Inspection of the sCD-MPR spectrum indicates that the receptor is dynamic in the absence of Man-6-P as evidenced by the heterogeneous peak intensities and line broadening observed for most of the resonances (Figure 5A). In contrast, binding of Man-6-P restricts the sCD-MPR to the open conformation as shown by the homogeneous peak intensities and line widths (Figure 5A). Additionally, a comparison of the sCD-MPR and EQKM spectra collected in the absence of Man-6-P revealed that the peaks in the spectrum overlay well, suggesting that EQKM can adopt the closed conformation similar to that of the sCD-MPR (Figure 5A). Titrations of ^{15}N-labeled sCD-MPR or ^{15}N-labeled EQKM with Man-6-P were monitored by $^{15}N-^{1}H$ HSQC spectroscopy to identify amino acid residues that experienced chemical shift changes upon Man-6-P binding. Although chemical shift assignments have not yet been made, relative chemical shift changes were monitored for three different backbone amides

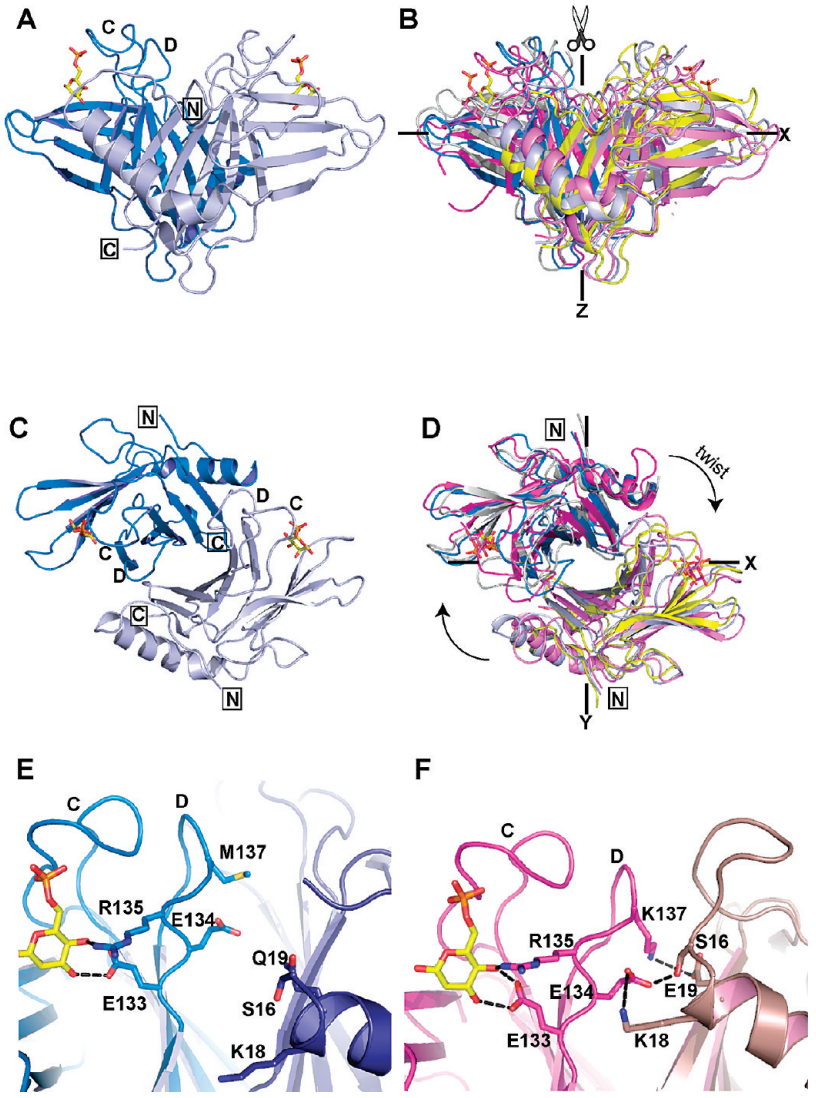

FIGURE 4: Comparison of the dimer structures of sCD-MPR in the absence and presence of Man-6-P with that of EQKM/Man-6-P. (A) The Man-6-P-bound structure of EQKM (PDB entry 3K41, blue and gray) was overlaid (B) with the structures of sCD-MPR crystallized in the unbound state (PDB entry 2RL7, gray and yellow) as well as bound to Man-6-P (PDB entry 2RL8, magenta and pink). (C and D) The dimers have been rotated down 90° from the views in panels A and B, respectively, showing the superimposition looking down the *Z* axis. Close-up views showing the dimer interface of (E) EQKM/Man-6-P (PDB entry 3K41) and (F) sCD-MPR (PDB entry 2RL8). Residues on loop D proposed to interact with either the ligand or loop N of the other monomer are shown. Black dashed lines indicate potential hydrogen bond or salt bridge interactions. Loops C and D are indicated in panels A, C, E, and F. The N- and C-termini are boxed in panels A, C, and D. The location of Man-6-P (yellow ball and stick) is shown.

for sCD-MPR, and two different backbone amides as well as the side chain amide of Gln19 for EQKM. Nonlinear fitting of the chemical shift changes as a function of Man-6-P concentration yielded apparent K_d values of ~1 and ~150 mM for sCD-MPR and EQKM, respectively (Figure 5B). These results demonstrate that EQKM binds Man-6-P with an ~150-fold lower affinity than the wild-type receptor, which is consistent with the data obtained by SPR analyses (Figure 2).

Crystal Structure of EQKM in the Absence of Man-6-P. Given the observed differences in the quaternary structure of EQKM bound to Man-6-P (Figure 4B,D), we sought to obtain the structure of EQKM in a ligand-free form by crystallizing the protein in the absence of Man-6-P at pH 6.5. The resulting structure was found to contain a sulfate ion in the ligand binding cavity near the position at which the phosphate moiety of Man-6-P would reside (Figure 6B). The presence of sulfate was due to the crystallization conditions in which 3 M ammonium sulfate was used as the precipitant. The protein was crystallized at a higher pH (pH 7.0) in an attempt to deprotonate His105 (which coordinates the phosphate group) to eliminate binding of the sulfate ion. However, both resulting structures were essentially identical with an rms deviation of 0.17 Å, and in both structures, the residues within loop D were disordered in one of the two monomers. Therefore, detailed structural analysis was conducted for the structure crystallized at pH 7.0 (EQKM/sulfate). Interestingly, although the relative orientation of the monomers of this sulfate-bound structure is the same as that found in EQKM/Man-6-P, the well-defined monomer demonstrates some intriguing differences that have not been seen in any of the sCD-MPR structures determined to date. The major difference resides in the conformation of loop D. Our previous structures of sCD-MPR (*10*, *12*) demonstrated that in the ligand-free state loop D pivots into the carbohydrate binding site and establishes a network of hydrogen bond interactions which preserve the orientation of three (Gln66, Arg111, and Tyr143) of the four essential binding site residues: only the position of Glu133 is

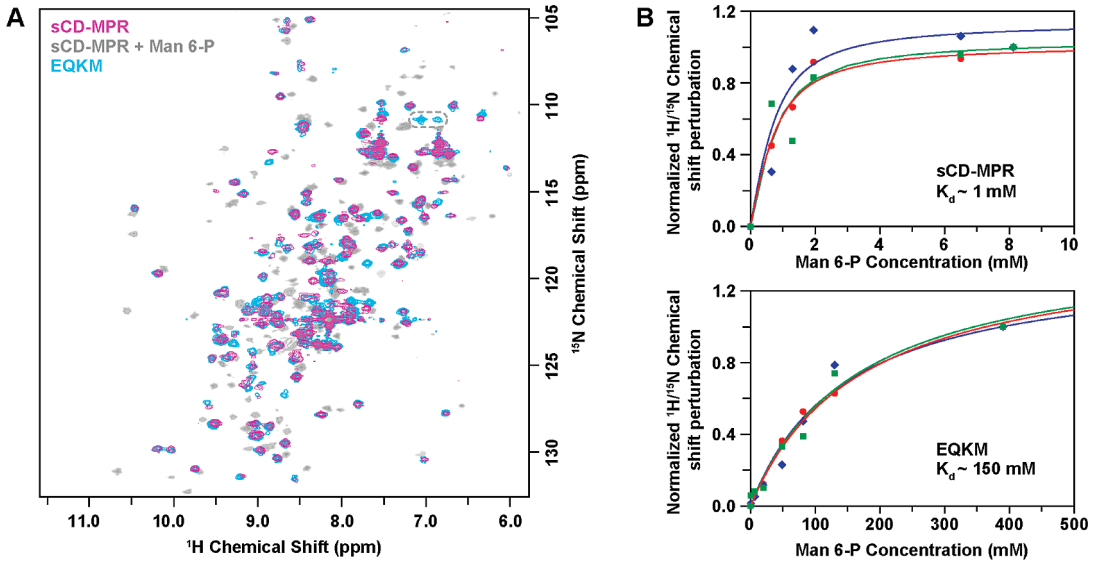

FIGURE 5: Effect of elimination of the intermonomer salt bridge (Glu19−Lys137) on the solution structure and Man-6-P binding affinity of sCD-MPR. (A) Overlay of ^{1}H−^{15}N HSQC spectra collected on sCD-MPR in the presence (gray) and absence (magenta) of Man-6-P. The ^{1}H−^{15}N HSQC spectrum of EQKM (cyan) collected in the absence of Man-6-P is shown for the sake of comparison. The side chain amide group (Gln19) of EQKM is indicated by the dashed gray circle. (B) Apparent binding affinities (K_d) were obtained by ^{1}H−^{15}N HSQC spectroscopy titrating Man-6-P with ^{15}N-labeled sCD-MPR or EQKM and monitoring chemical shift perturbations for three different nitrogen groups.

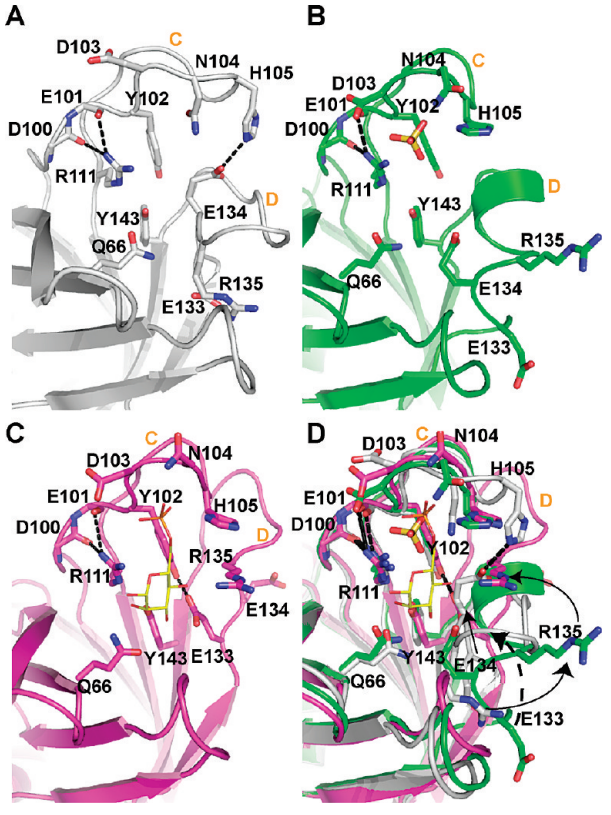

FIGURE 6: Close-up view of the binding site unoccupied, partially occupied, or fully bound to ligand. (A) In the complete absence of ligand, loop C is elongated to form a β-finger (sCD-MPR, PDB entry 2RL7). (B) However, loop C contracts in the presence of a sulfate ion (yellow ball and stick) (EQKM/sulfate, PDB entry 3K42). The presence of sulfate also results in the movement of loop D out of the binding pocket and the reordering of loop D to form an intermediate α-helix. (C) The occupation of both the phosphate and mannose binding regions of the receptor (sCD-MPR, PDB entry 2RL8) moves the residues of loop D to the side of the binding pocket. (D) Superimposition of all three states of the binding pocket. Residues are labeled as well as loops C and D in all four panels.

altered since it resides within loop D (Figure 6A). In contrast, in the presence of ligand, the N- and C-terminal residues of loop D form a side of the binding pocket near the mannose ring while the residues at the tip of the loop (encompassing Lys137) interact with residues in the N-terminal region of the adjacent monomer (including Glu19) (Figures 4F and 6C) (*10*, *12*). Importantly, these interactions form a direct link between ligand binding in one monomer and the N-terminal region of the other monomer (Figure 4F). The EQKM/sulfate structure reveals that the residues of loop D form one turn of an α-helix (Figure 6B). Although the significance of this short helical conformation is not entirely clear, the observation that loop D adopts a different conformation (either disordered or α-helical) (Figure 6B) suggests that this region of the receptor is highly mobile and its reordering plays a role in the dimer reorientation observed in response to the presence or absence of ligand.

The Presence of a Sulfate Ion in the Binding Site of EQKM/Sulfate Mimics an Intermediate Binding Site Conformation. The structure of the sCD-MPR under a variety of conditions (*10*−*12*, *28*) has provided insight into the mechanism of ligand binding and release. The binding pocket of CD-MPR is comprised of two functional regions: the phosphate binding area (composed of residues in loop C) and the mannose binding area (composed of residues from β-strands 3 and 4 of the front sheet as well as residues near the N- and C-termini of loop D). As described above, in the absence of ligand, loop D is positioned in the carbohydrate recognition site, and the residues of loop C also undergo movement relative to each other (Figure 6A), allowing for changes in the interplay between the two functional regions of the binding pocket. In the ligand-bound structures of the sCD-MPR (Figure 6C), Tyr102 is within hydrogen bonding distance of Glu133; however, the interaction of Glu133 shifts from Tyr102 to Arg135 in the ligand-free state (Figure 6A), and Glu134 of loop D is now in position to form a hydrogen bond to His105 of loop C (Figure 6A). The shifting of the hydrogen bonding pattern within the binding site (Figure 6A, C,D) allows the side chain of Asp103 (coordinates the cation

Mn^{2+}) to move out of the phosphate binding area, thus opening the cavity to allow subsequent access of a phosphate moiety. Taken together, these interactions serve to link the two regions of the binding pocket together.

The EQKM/sulfate structure captures a unique view of the relationship between the phosphate and mannose binding regions by allowing only half of the binding site to be occupied (i.e., the phosphate recognition region) (Figure 6B). In this location, it is possible for the sulfate ion to have electrostatic interactions with the side chain nitrogen atoms of His105, Asn104, and Lys73 (Figure 6B). Therefore, in terms of loop C, the EQKM/sulfate structure more closely resembles a bound structure. As previously reported for other bound and unbound structures, three of the four essential binding residues do not alter their position in the mannose binding area in the presence of sulfate. The residues in loop D (including Glu133), however, do not overlay with their counterparts in either the ligand-bound or ligand-free structures (Figure 6D); rather, their position suggests a possible intermediate state between the ligand-bound and ligand-free states.

Monomer Reorientation and the Dimer Interface in the Presence or Absence of Ligand. As described above, the structure of sCD-MPR is dynamic and undergoes a series of transitions as ligand is bound and released, with the presence of ligand necessitating the movement of loop D residues out of the region occupied by the mannose ring (Figure 6). In addition, changes in quaternary structure occur that can be described as a scissoring and twisting motion of one monomer relative to the other (Figure 4B,D), resulting in changes in association between residues of the dimer interface. We have captured four states along this pathway of ligand binding: ligand-free, closed dimer conformation (state 1, wild-type sCD-MPR, PDB entry 2RL7); partial occupancy, in which only the phosphate portion of the binding pocket is filled and has an intermediate dimer conformation (state 2, EQKM/sulfate, PDB entry 3K42); both phosphate and carbohydrate regions of the binding site occupied with an intermediate dimer conformation (state 3, EQKM/Man-6-P, PDB entry 3K41); and ligand-bound, open dimer conformation (state 4, wild-type sCD-MPR, PDB entry 2RL8). The dimer interface is comprised of two regions: (1) the interactions between loop N and loop D which are present only when ligand is present and (2) a set of core residues involved in monomer−monomer interactions that are present in both the ligand-free and ligand-bound conformations. This core region consists of hydrophobic and hydrophilic interactions between residues located in the C-terminal β-sheets as well as ionic interactions between residues near loop C of one monomer and loop D of the other. A comparison of the ligand-unbound structure (state 1) and the partially occupied binding pocket (state 2) reveals that these interface residues adopt essentially the same orientation, with the exception of Ser132 (located on the C-terminus of strand 8 leading into loop D) and Asp140 (within loop D) (Figure 7A). The formation of the helical turn in loop D results in a 1.9 Å repositioning of the Cα atoms of Asp140, while the Cα atoms of Ser132 differ by ~4 Å. The presence of the sulfate ion forces the residues of loop C into a bound conformation, while the residues in loop D are left in an intermediate or transitional position. Addition of mannose to the binding pocket (Figure 7B, state 3) continues the movement of Asp140, and rotation of Phe142 is now observed. Comparison of both of these sets of structures reveals that backbone and side chain movements are fairly well confined to the area of the interface nearest loop D (Figure 7A,B, circled region). The relocation of the residues in loop D to form the binding pocket places Asp140 in a region of concentrated positively charged residues, including Lys97 and Arg112 (Figure 7G). The EQKM/Man-6-P structure reveals that Asp140 of one monomer is within ~6 Å of its counterpart in the other monomer (Figure 7G). This juxtapositioning of negative charge may serve to destabilize this dimer conformation in this mutant form of the receptor (EQKM), thus contributing to its much lower (~150-fold) affinity for ligand. The final step in formation of the fully ligand-bound wild-type structure, with both regions of the binding site fully occupied (Figure 7C, state 4), produces additional side chain rearrangements. However, these rearrangements are now localized to the N-terminal side of the interface and involve Gln84, Phe86, and Trp91. Comparison of these different structures illustrates the dynamic nature of the CD-MPR.

Conclusions and Future Studies. The CD-MPR travels between various cellular compartments and must undergo conformational changes between ligand-bound and unbound states during the loading and unloading of its cargo. We now have structures of sCD-MPR in four different conformations representing different stages of ligand binding: the wild-type ligand-free structure (*12*) (PDB entry 2RL7), EQKM/sulfate (this work) (PDB entry 3K42), EQKM/Man-6-P (this work) (PDB entry 3K41), and the wild-type fully bound structure (*12*) (PDB entry 2RL8). Thus, we are now in a position to better understand the individual steps involved in the interconversion of the ligand-free and ligand-bound states of the CD-MPR. When the CD-MPR is in the ligand-free state (state 1), the receptor adopts the closed form in which loop D folds into the mannose binding site to interact with the residues that bind the sugar ring, thereby preserving the conformations of the sugar binding residues. The intermonomer interactions between loops N (E19) and D (K137) are not present in this conformation. State 2 of the receptor is represented by the occupation of the phosphate binding region by the analogous tetrahedral sulfate anion. Although this state is artificial since the natural ligand would also have a carbohydrate moiety attached to the phosphate, it allows us to decouple the binding of carbohydrate from that of the phosphate group, thereby providing information about an intermediate state of binding by the receptor. When the phosphate moiety of the ligand binds to the receptor, loop C, including Asp103, Asn104, and His105, reconfigures and accommodates the phosphate of the ligand as seen in the structure of EQKM/sulfate. When loop C is reordered, the interactions between it and the rest of the binding pocket are altered. These alterations may facilitate the movement of loop D out of the binding pocket through a series of reordering steps (one being the α-helical conformation captured in the EQKM/sulfate structures). The partial occupation of the binding site is accompanied by changes in the dimer to the intermediate state. In the third state of the receptor (EQKM/Man-6-P), both the phosphate and the carbohydrate recognition regions of the binding site are occupied and the four residues essential to carbohydrate recognition are in place. However, in this state, the receptor has not achieved optimal dimer orientation for maximal binding affinity. Further reorientation of the monomers occurs in the fourth state (representing the highest-affinity state) to optimize intermonomer interactions. As demonstrated by the characterization of the EQKM mutant presented in this work, these intermonomer interactions, including the salt bridge between Glu19 of one monomer and K137 of the other, prove to be critical for the receptor to attain high-affinity ligand binding.

It has been shown that the loading and unloading of its cargo are facilitated by changes of pH in each subcellular compartment

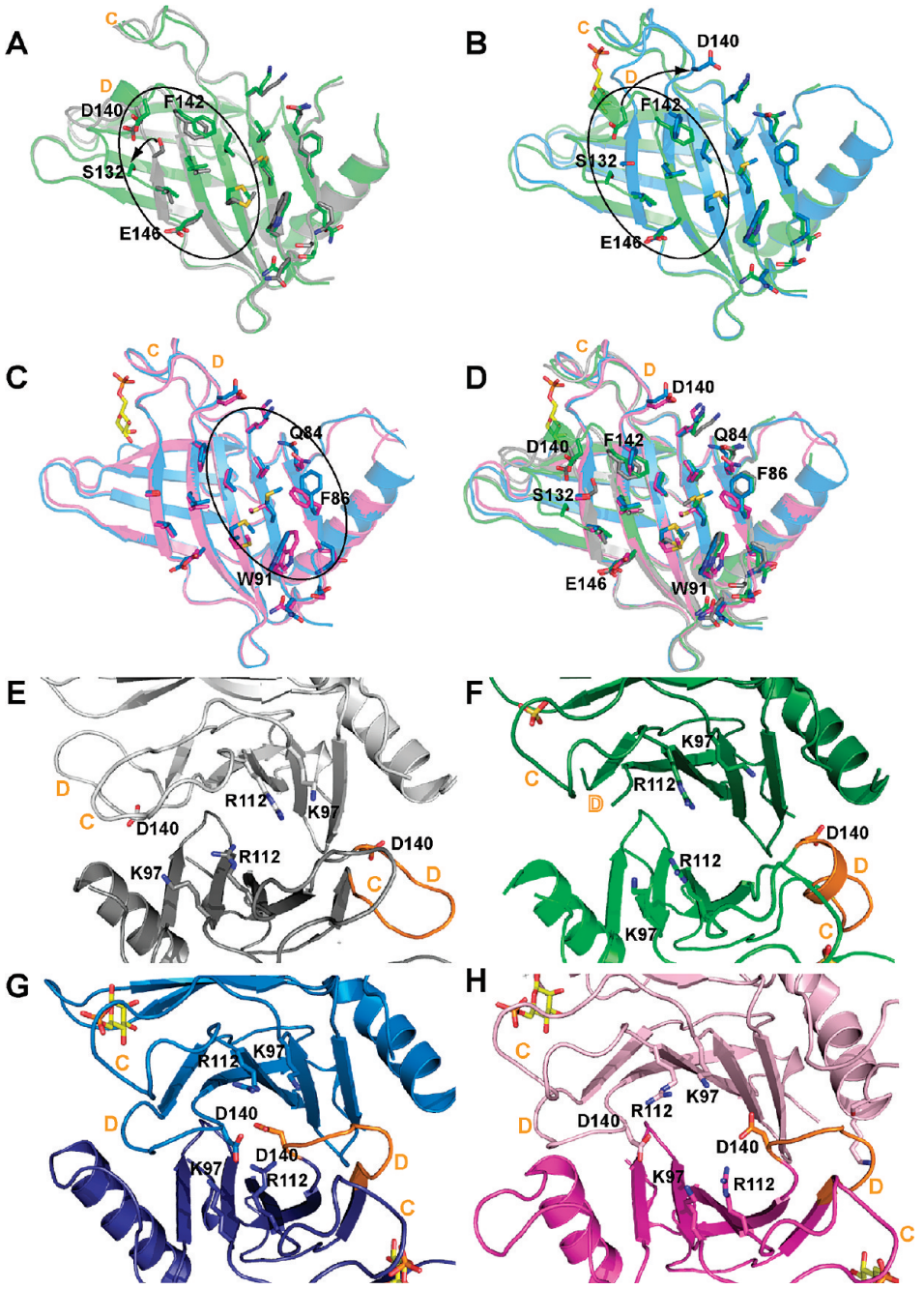

FIGURE 7: Mapping the changes in the dimer association for the four states of sCD-MPR. (A) Overlay of the unbound (PDB entry 2RL7, gray) and partially bound (PDB entry 3K42, green) receptor. The occupation of the phosphate binding region by sulfate (green) is accompanied by reordering of residues of loop D which displaces Ser132 from β-strand 8 while causing more minor perturbations in the locations of Asp140 (unbound sCD-MPR, gray, PDB entry 2RL7). (B) Overlay of the partially bound (PDB entry 3K42, green) and fully bound (PDB entry 2RL8, blue) mutant receptor. The presence of Man-6-P (EQKM/Man-6-P, PDB entry 3K41, blue) results in the complete transition of loop D to that found in the fully bound structure. (C) Overlay of the Man-6-P-bound mutant (PDB entry 3K41, blue) and wild-type (PDB entry 2RL8, pink) receptors. The final dimer transition following binding of ligand (PDB entry 2RL8, bound) involves shifting of the side chains closest to the N-terminal loop. (D) Overlay of all monomers. In panels A−C, residues proposed to be involved in the transition from the unbound to bound states are circled. For the sake of clarity, the dimers were rotated downward 90° from panels A−D to show the electrostatic interactions near loops C and D of the dimer in (E) the unbound form (PDB entry 2RL7), (F) the partially bound form (i.e., phosphate portion of the binding site occupied with sulfate) (EQKM/sulfate, PDB entry 3K42), (G) Man-6-P bound in absence of the Glu19−Lys137 salt bridge (EQKM/Man-6-P, PDB entry 3K41), and (H) sCD-MPR (PDB entry 2RL8). Loops C and D are labeled in orange in all panels.

in which the CD-MPR travels (*29*). However, it is not clear which region or residue(s) of the CD-MPR is responsible for sensing these pH changes. We have hypothesized Glu133 (one of the ligand binding residues in loop D) and the phosphate moiety of Man-6-P are responsible for responding to the pH changes for unloading the ligand (*12*). However, there are other candidates that might act as the pH sensor(s), including His105 in loop C (binds to phosphate), Glu134 in loop D, Glu19 near the N-terminus, and Glu146 near the hydrophobic interface. Future studies using NMR and EPR spectroscopic analyses will be required to fully evaluate the dynamic nature of the CD-MPR, to assess its allosteric behavior, and to identify the residues involved in pH-dependent ligand binding.

ACKNOWLEDGMENT

The BIAcore 3000 instrument (Protein and Nucleic Acid Core Facility, Medical College of Wisconsin) was purchased through a grant from the Advancing a Healthier Wisconsin program.

REFERENCES

1. Kornfeld, S., and Mellman, I. (1989) The biogenesis of lysosomes. *Annu. Rev. Cell Biol. 5*, 483–525.
2. Ghosh, P., Dahms, N. M., and Kornfeld, S. (2003) Mannose 6-phosphate receptors: New twists in the tale. *Nat. Rev. Mol. Cell Biol. 4*, 202–213.
3. Dahms, N. M., Olson, L. J., and Kim, J. J. (2008) Strategies for carbohydrate recognition by the mannose 6-phosphate receptors. *Glycobiology 18*, 664–678.
4. Braulke, T., and Bonifacino, J. S. (2009) Sorting of lysosomal proteins. *Biochim. Biophys. Acta 1793*, 605–614.
5. Arighi, C. N., Hartnell, L. M., Aguilar, R. C., Haft, C. R., and Bonifacino, J. S. (2004) Role of the mammalian retromer in sorting of the cation-independent mannose 6-phosphate receptor. *J. Cell Biol. 165*, 123–133.
6. Stein, M., Zijderhand-Bleekemolen, J. E., Geuze, H., Hasilik, A., and von Figura, K. (1987) Mr 46,000 mannose 6-phosphate specific receptor: Its role in targeting of lysosomal enzymes. *EMBO J. 6*, 2677–2681.
7. Watanabe, H., Grubb, J. H., and Sly, W. S. (1990) The overexpressed human 46-kDa mannose 6-phosphate receptor mediates endocytosis and sorting of β-glucuronidase. *Proc. Natl. Acad. Sci. U.S.A. 87*, 8036–8040.
8. Tong, P. Y., and Kornfeld, S. (1989) Ligand interactions of the cation-dependent mannose 6-phosphate receptor. Comparison with the cation-independent mannose 6-phosphate receptor. *J. Biol. Chem. 264*, 7970–7975.
9. Qian, M., Sleat, D. E., Zheng, H., Moore, D., and Lobel, P. (2008) Proteomics analysis of serum from mutant mice reveals lysosomal proteins selectively transported by each of the two mannose 6-phosphate receptors. *Mol. Cell. Proteomics 7*, 58–70.
10. Olson, L. J., Zhang, J., Dahms, N. M., and Kim, J.-J. P. (2002) Twists and turns of the CD-MPR: Ligand-bound versus ligand-free receptor. *J. Biol. Chem. 277*, 10156–10161.
11. Roberts, D. L., Weix, D. J., Dahms, N. M., and Kim, J.-J. P. (1998) Molecular basis of lysosomal enzyme recognition: Three-dimensional structure of the cation-dependent mannose 6-phosphate receptor. *Cell 93*, 639–648.
12. Olson, L. J., Hindsgaul, O., Dahms, N. M., and Kim, J. J. (2008) Structural Insights into the Mechanism of pH-dependent Ligand Binding and Release by the Cation-dependent Mannose 6-Phosphate Receptor. *J. Biol. Chem. 283*, 10124–10134.
13. Sun, G., Zhao, H., Kalyanaraman, B., and Dahms, N. M. (2005) Identification of residues essential for carbohydrate recognition and cation dependence of the 46-kDa mannose 6-phosphate receptor. *Glycobiology 15*, 1136–1149.
14. Zhang, Y., and Dahms, N. M. (1993) Site-directed removal of N-glycosylation sites in the bovine cation- dependent mannose 6-phosphate receptor: Effects on ligand binding, intracellular targetting and association with binding immunoglobulin protein. *Biochem. J. 295*, 841–848.
15. Olson, L. J., Hancock, M. K., Dix, D., Kim, J.-J. P., and Dahms, N. M. (1999) Mutational analysis of the binding site residues of the bovine cation-dependent mannose 6-phosphate receptor. *J. Biol. Chem. 274*, 36905–36911.
16. Marron-Terada, P. G., Brzycki-Wessell, M. A., and Dahms, N. M. (1998) The two mannose 6-phosphate binding sites of the insulin-like growth factor-II/mannose 6-phosphate receptor display different ligand binding properties. *J. Biol. Chem. 273*, 22358–22366.
17. Myszka, D. G. (2000) Kinetic, equilibrium, and thermodynamic analysis of macromolecular interactions with BIACORE. *Methods Enzymol. 323*, 325–340.
18. McPherson, A. (1990) Current approaches to macromolecular crystallization. *Eur. J. Biochem. 189*, 1–23.
19. Otwinowski, Z., and Minor, W. (1997) Processing of X-ray diffraction data collected in oscillation mode. *Methods Enzymol. 276*, 307–326.
20. Collaborative Computational Project, Number 4 (1994) The CCP4 suite: Programs for protein crystallography. *Acta Crystallogr. D50*, 760–763.
21. Potterton, L., McNicholas, S., Krissinel, E., Gruber, J., Cowtan, K., Emsley, P., Murshudov, G. N., Cohen, S., Perrakis, A., and Noble, M. (2004) Developments in the CCP4 molecular-graphics project. *Acta Crystallogr. D60*, 2288–2294.
22. Brunger, A. T., Adams, P. D., Clore, G. M., DeLano, W. L., Gros, P., Grosse-Kunstleve, R. W., Jiang, J.-S., Kuszewski, J., Nilges, M., Pannu, N. S., Read, R. J., Rice, L. M., Simonson, T., and Warren, G. L. (1998) Crystallography & NMR System: A New Software Suite for Macromolecular Structure Determination. *Acta Crystallogr. D54*, 905–921.
23. Roussel, A., and Cambillau, C. (1994) TURBO-FRODO. The Manual , version 4.2, Biographics LCCMB, Marseille, France.
24. Delaglio, F., Grzesiek, S., Vuister, G. W., Zhu, G., Pfeifer, J., and Vax, A. (1995) NMRPipe: A multidemensional spectral processing system based on UNIX pipes. *J. Biomol. NMR 6*, 277–293.
25. Seibert, C., Veldkamp, C. T., Peterson, F. C., Chait, B. T., Volkman, B. F., and Sakmar, T. P. (2008) Sequential tyrosine sulfation of CXCR4 by tyrosylprotein sulfotransferases. *Biochemistry 47*, 11251–11262.
26. Reddy, S. T., and Dahms, N. M. (2002) High-level expression and characterization of a secreted recombinant cation-dependent mannose 6-phosphate receptor in *Pichia pastoris*. *Protein Expression Purif. 26*, 290–300.
27. Ma, Z. M., Grubb, J. H., and Sly, W. S. (1991) Cloning, sequencing, and functional characterization of the murine 46- kDa mannose 6-phosphate receptor. *J. Biol. Chem. 266*, 10589–10595.
28. Olson, L. J., Zhang, J., Lee, Y. C., Dahms, N. M., and Kim, J.-J. P. (1999) Structural basis for recognition of phosphorylated high mannose oligosaccharides by the cation-dependent mannose 6-phosphate receptor. *J. Biol. Chem. 274*, 29889–29896.
29. Imort, M., Zuhlsdorf, M., Feige, U., Hasilik, A., and von Figura, K. (1983) Biosynthesis and transport of lysosomal enzymes in human monocytes and macrophages. Effects of ammonium chloride, zymosan and tunicamycin. *Biochem. J. 214*, 671–678.